

JGR Space Physics

RESEARCH ARTICLE

10.1029/2020JA027773

Key Points:

- Effect of the bottom-side density gradient of postsunset F layer on equatorial spread F development is discussed using Digisonde data
- Comparison of the results during solar minimum and maximum epochs reveal a large degree of dependence of plasma bubble on solar flux
- A larger density gradient of the F layer bottom-side during low solar flux is responsible for an enhanced Raleigh-Taylor instability growth

Correspondence to:

M. A. Abdu,
abdu.manga@gmail.com

Citation:

Abdu, M. A., Kherani, E. A., & Sousasantos, J. (2020). Role of bottom-side density gradient in the development of equatorial plasma bubble/spread F irregularities: Solar minimum and maximum conditions. *Journal of Geophysical Research: Space Physics*, 125, e2020JA027773. <https://doi.org/10.1029/2020JA027773>

Received 10 JAN 2020

Accepted 17 AUG 2020

Accepted article online 20 AUG 2020

Role of Bottom-Side Density Gradient in the Development of Equatorial Plasma Bubble/Spread F Irregularities: Solar Minimum and Maximum Conditions

M. A. Abdu¹ , E. A. Kherani¹ , and J. Sousasantos²

¹Instituto Nacional de Pesquisas Espaciais, São José dos Campos, Brazil, ²Instituto Tecnológico de Aeronáutica, São José dos Campos, Brazil

Abstract From the analysis of Digisonde data over Brazilian equatorial and low-latitude sites, we investigate the relative importance of the different parameters driving the generation of rising bubble-type and bottom-type spread F (SF) irregularities. Data for the complete month of October 2001, a solar maximum epoch ($F_{10.7} = 210$), and that of October 2008, an extended solar minimum period ($F_{10.7} = 70$), are analyzed to examine the SF intensity and occurrence rate as a function of the evening prereversal vertical drift velocity and the corresponding F layer heights and the bottom-side density gradient. While the SF at the equatorial site is indicative of both the bottom-side irregularities and rising bubbles, the SF at the low latitude represents exclusively the latter. Comparison of the results, from the two epochs, reveals a large decrease in the intensity and occurrence rate of plasma bubbles, with a decrease in solar flux. But a notable increase in these characteristics is observed in the case of bottom-side SF. It is found that a larger (steeper) density gradient of the F layer bottom side that exists in the low solar flux condition is responsible for an enhanced Raleigh-Taylor instability growth, counterbalancing a reduction in this rate that may arise from a smaller prereversal vertical drift and lower layer height that also characterize the low solar flux condition. Thus, the role of the bottom-side density gradient in the ESF instability growth has been identified for the first time in terms of its ability to explain the contrasting irregularity features as observed during solar flux maximum and minimum years.

1. Introduction

The equatorial plasma bubbles (EPBs), widely known as equatorial spread F (ESF) irregularities, of the nighttime equatorial ionosphere have been the subject of extensive investigation since the first study of the range spreading F layer echo traces in the postsunset ionograms over Huancayo conducted by Booker and Wells (1938). Investigations of the ESF/EPB irregularities have been conducted for the last several decades using a wide variety of diagnostic techniques, both ground based and space borne, and model simulation studies. The results of such investigations have established the outstanding characteristics of these irregularities in the form of their generation mechanisms, global distribution, and morphology (e.g., see Abdu et al., 1981; Farley et al., 1970; Fejer et al., 1999; Huang & Kelley, 1996; Ossakow et al., 1979; Rastogi & Woodman, 1978; Tsunoda, 1981; Woodman & La Hoz, 1976; Zalesak et al., 1982) and their contribution to ionospheric scintillation (e.g., see Alfonsi et al., 2013; Shi et al., 2011; Wang et al., 2014).

The ESF/EPB irregularities cover a wide range of spatial scales with their occurrence exhibiting significant variability at wide-ranging time scales. The generation of the EPB through the Raleigh-Taylor (R-T) instability mechanism can be explained as follows: In the presence of a perturbation at the upward gradient region of the ionization boundary, the action of gravity generates an eastward ion current, which could induce a polarization electric field, E . The polarity of the E is eastward (westward) in the reduced (enhanced) density regions so that the $E \times B$ vertical drift of the ions and electrons is upward (downward) in the lower (higher) density regions of the perturbation. As the plasma in the reduced density region rises up, the amplitude of the reduction relative to the upward increasing background plasma density increases, which results in an increase in the eastward polarization electric field that causes the accelerated upward motion of the rarified plasma, leading to a further increase in the polarization electric field and associated enhanced vertical drift, a process resulting in nonlinear growth of the instability. This process results in the formation of magnetic field-aligned plasma depleted regions, widely known as plasma bubbles. From the equations of continuity

and current convergence, the local growth rate of the instability, in its simplified form, is given by (Ossakow, 1981)

$$\gamma_L = \Delta n/n\{g/\nu_{in}\} - \beta_L \quad (1)$$

where n is the electron density, β_L is the recombination rate, and ν_{in} is the ion-neutral collision frequency.

In the growth phase, the walls of these EPBs are characterized by large density gradients that become unstable to perturbations in density and polarization electric field, as a result of which secondary irregularities may develop through cascading processes, leading to formations of irregularities of scale sizes ranging from a few meters to several hundreds of kilometers (e.g., see Haerendel et al., 1992). The composite characterization of these structures is widely known by the generic name, equatorial spread F irregularities, or, simply, ESF.

Based on existing data sets and the available results of investigations, we now have a fairly good knowledge and predictive capability on the long- to medium-term variability of the ESF/EPB phenomenon. In contrast to this, our understanding of the variabilities at short and day-to-day time scales continues to be very limited mainly because of the lack of the needed information on the related short-term variability of the background ionospheric and atmospheric conditions that basically control the ESF development process (i.e., the initiation and evolution of the irregularities). It is now well recognized that the ESF irregularities are produced by a plasma instability process, widely believed to be the R-T mechanism or, equivalently, the gradient drift mechanism, operating at the bottom-side gradient region of the F layer that may typically rise to large heights in the postsunset hours. The rapid uplift of the post-sunset F layer is due to the enhanced plasma vertical drift driven by the evening enhancement of the zonal (eastward) electric field, known as the prereversal electric field (PRE). The PRE is generated through the action of the F layer dynamo driven by the thermospheric zonal wind, which is eastward in the evening, and under the presence of the sunset decay in the E layer Pedersen conductivity (Farley et al., 1986; Heelis et al., 1974; Rishbeth, 1971). The instability growth at the F layer bottom side has its source in a seed perturbation in electron density and polarization electric field produced by the perturbation winds that are associated with upward propagating gravity waves. The gravity waves are believed to be originating in large part, presumably, from a tropospheric convection process associated with the Intertropical Convergence Zone (Fritts et al., 2009; Li et al., 2016; McClure et al., 1998; Tsunoda, 2010). Thus, the basic key parameters controlling the ESF/bubble development may be considered as (1) the evening vertical drift enhancement (due to the PRE) and the resulting F layer uplift to sufficiently large heights; (2) the F layer bottom-side density gradient that becomes steeper in the post-sunset hours; and (3) a source of density perturbation in the form of gravity waves, or a velocity shear in zonal plasma drift (Hysell et al., 2005) acting as a seed, to initiate the instability growth. Once initiated under a sufficiently large linear growth rate by the R-T mechanism, the instability may grow nonlinearly to the topside ionosphere, leading to the formation of flux tube-aligned plasma depletions (or plasma bubbles), extending (north and south) their extremities to low latitudes (Tsunoda, 1981). The strength of an irregularity can be represented by a parameter, f_{op} , the top frequency of the spread F (SF) trace in the ionogram (Abdu et al., 2012). This is based on the fact that the cascading into smaller scale sizes produces larger f_{op} , which is an indication that the irregularities grow stronger. The instability growth may, however, become retarded/limited due to the field line-integrated Pedersen conductivity that is controlled by thermospheric meridional winds (Maruyama, 1988). The structuring of the irregularities in wide-ranging temporal and spatial scales, typically associated with the plasma bubble development, is the subject of ongoing investigations using a wide variety of diagnostic tools (including radio, optical, remote, and in situ techniques) and simulation studies.

Large degrees of the variability at relatively short time scales may occur in the background ionosphere that controls the parameters driving the instability process that are responsible for the widely observed short-term variability in the irregularity occurrence even under magnetically quiet conditions. In recent years, several studies have been realized in efforts to understand the cause-effect connections in the ESF variability at different time scales that can be identified, or associated, with any one or more of the specific parameters listed above. The most widely discussed aspects have so far been that concerning the role of vertical drift and/or that of F layer height rise on the ESF irregularity development (e.g., see Abdu et al., 1983, 2009; Farley et al., 1970; Fejer et al., 1999; Jayachandran et al., 1993; Kil et al., 2009; Su et al., 2008). In recent years, the role of a precursor seeding mechanism due to gravity wave perturbations, and possible sources of

such gravity waves, have also been extensively investigated with increasing focus (Abdu et al., 2015; Fritts et al., 2009; Huang & Kelley, 1996; Kherani et al., 2011; Li et al., 2016; McClure et al., 1998; Takahashi et al., 2009; Tsunoda, 2010; Tulasi Ram et al., 2014). Other possible sources of ESF irregularity initiations that have been discussed are those related to the collisional shear instability, postsunset plasma flow vortex, and thermospheric winds (Hysell et al., 2005; Kudeki et al., 2007; MacDougall et al., 1998).

It is to be noted that the basic precursor conditions of the background ionosphere, that is, the vertical plasma drift, the layer height, and the bottom-side gradient, conducive or not to EPB/ESF development, are interdependent parameters, as will be discussed below. While a great deal of understanding has been achieved about the control of the vertical drift and layer height on the ESF development (as per the above cited references and many others not cited here), very little (or almost nothing) is known observationally on the specific role of bottom-side density gradient on the ESF development. Nevertheless, a model simulation study (Huang & Kelley, 1996) has shown the significant influence of the bottom-side density gradient on the instability growth rate by the R-T mechanism, in the sense that an increase in this gradient (i.e., a decrease in the scale length of the gradient) could cause a corresponding increase in the growth rate. Such a dependence is evident from the instability linear growth rate expressions, a version of which, based on field line-integrated parameters (Sultan, 1996), is given by

$$\gamma_{FT} = (\Sigma^{E,F}/\Sigma^F + \Sigma^E) \{E/B - U_{FT}^P + g/\nu_{eff}\} / L_{FT} - \beta_{FT} \quad (2)$$

Here, γ_{FT} is the growth rate based on flux tube-integrated parameters; $\Sigma^{E,F}$ is the field line-integrated Pedersen conductivities for the E and F region segments of a field line; U_{FT}^P is the conductivity-weighted flux tube-integrated vertical wind; β_{FT} is the recombination loss rate; ν_{eff} is the effective ion-neutral collision frequency; and L_{FT} is the field line-integrated F layer bottom-side density gradient scale length. The subscript “FT” in Equation 2 stands for flux tube-integrated quantity. The inverse relationship between the bottom-side density gradient scale length L_{FT} and the instability linear growth rate γ_{FT} is clear from Equation 2. In this paper we will demonstrate the specific role played by the bottom-side density gradient in shaping the EPB/ESF intensity and occurrence rates, highlighting their relative importance during solar maximum and minimum years. Observational results will be verified/supported using numerical modeling experiments simulating the R-T instability growth under realistic control parameters representative of the observational data. Toward accomplishing this objective, we will consider also the roles of the evening PRE vertical drift and gravity waves oscillations in comparison to the roles of the bottom-side gradient, in shaping the ESF variations.

Digisonde data for October 2001, a solar maximum epoch (with average $F_{10.7} = 200$) and for October 2008, a solar minimum epoch (with average $F_{10.7} = 70$), are used in the analysis. SF intensity and occurrence rate over Fortaleza (FZA0M), a near equatorial station (3.9°S, 38.45°W, dip angle: -9°), are compared with corresponding data over a low-latitude station, Cachoeira Paulista (CAJ2M) (22.6°S, 315°E; dip angle: -28°) during the October months of 2001 and 2008. Further, the characteristics of the evening PRE vertical drift, and the F layer height oscillations (presumably produced by gravity waves) over FZA0M, are compared between solar maximum and minimum epochs, in the attempt to identify/isolate the role of bottom-side gradient in the ESF development. Some published results on conjugate point observational results on SF will also be used in the analysis.

2. Observational Results

First, we will briefly recall some results of previous studies on the role of the PRE vertical drift in the irregularity growth beginning as bottom-side SF and developing to topside bubble irregularities. Based on the radar observations of SF over Jicamarca (Fejer et al., 1999) and ionosonde/Digisonde observations at equatorial and low-latitude sites (including at conjugate points) in Brazil (Abdu et al., 1983, 2009), it is known that a relatively smaller PRE vertical drift typically corresponds to bottom-side (or bottom-type) SF irregularities with limited or no growth to the topside ionosphere (i.e., the irregularities are restricted to the equatorial region). On the other hand, a relatively larger vertical drift (usually on the order of 30 m/s or higher) is necessary to produce field-aligned plasma depletion structures, that is, bubble-type SF irregularities, that

rise up to large heights over the equatorial topside ionosphere, extending their extremities to the low-latitude north and south conjugate points. They have been investigated by ground-based radars, Digisondes/ionosondes, optical imagers, and satellite borne sensors (e.g., see Abdu et al., 2009; Kil et al., 2006; Otsuka et al., 2002). From COPEX (Conjugate Point Equatorial Experiment) observations (Abdu et al., 2009; see also Abdu et al., 1983), it has been found that: (1) the delay Δt (by up to a few tens of minutes) in SF onsets at two magnetic conjugate sites, relative to the onset over the dip equator, corresponded to the vertical rise velocity (by a few hundreds of meters per second) of the field-aligned bubble structures over the equator; and further, (2) the time of initial SF onset over the equator as well as the Δt are found to be broadly dependent on the peak velocity of the PRE vertical drift. Thus, the value of the ratio E/B , which is a dominant factor in the linear growth rate, can be used as a rough criterion for a gross prediction of the bubble irregularity occurrence in a given situation. But such a prediction result would also reflect the degree to which the other factors in Equation 2, such as the bottom-side density gradient scale length L_{FT} and the g/ν_{eff} terms, that depend also upon the vertical drift may have additionally contributed to the result. The gravity term (g/ν_{eff}) is directly dependent on the vertical drift in the sense that it gains importance with the height increase that accompanies any vertical drift (see Sultan, 1996). The parameter L_{FT} (in Equation 2) is positively dependent on E/B . For example, a rise in the F layer height (due to an increase in E/B) normally involves a vertical extension of the layer, and hence an increase in L_{FT} (the scale length of the layer bottom side). However, the variation in the linear growth rate from low to high solar activity period is controlled more by the corresponding variation in the g/ν_{eff} term (in Equation 2) than by the other factors (E/B and U_{FT}^P). In this way, it becomes possible to identify (and evaluate) the specific role of the bottom-side density gradient in shaping the SF development and intensity, by comparing the contrasting SF behavior during low and high solar flux years, as will be discussed below.

With the above perspective, we will now examine the SF occurrence and intensity distributions over Fortaleza (3.9°S, 38.45°W, dip angle: -9°), an equatorial site, and CAJ2M (22.6°S, 315°E; dip angle: -28°), a low-latitude site, for the solar maximum epoch of October 2001 plotted in Figure 1 (top row). We may note that the ESF over FZA0M begins at around 21:30 UT (18:30 LT) on average (dashed line), with the onset time presenting significant day-to-day variability and a small gradual delay with increasing day number during the sampled period, whereas its average onset time over CAJ2M is delayed, occurring around 22:30 UT (19:30LT). The day-to-day variability in the SF onset time is caused by a corresponding variability in the conditions responsible for its development, the main factor being the F layer height at postsunset hours attaining a threshold limit required for instability initiation and growth. Some cases of very late occurrence of the SF in Figure 1 may also be attributed to this factor. We may note here that the observational cadence of the data is 10 min. The delay in the ESF occurrence over CAJ2M, with respect to that over FZA0M, is due to the time it takes for the field-aligned bubble growing upward over the equator to attain an altitude from where it can be mapped to the low-latitude F region over CAJ2M. Therefore, this delay can be considered to represent the bubble rise velocity, which for this period comes out to be on an average around 150 m/s. Similar plots for the solar minimum epoch of October 2008 are shown in Figure 1 (bottom row). We may note that the average local time of ESF initiation over FZA0M during solar minimum is around 19:00 LT (22:00 UT), which is, on average, 30 min later than that in solar maximum epoch. Also, during the solar minimum epoch, the ESF/plasma bubble onset time over CAJ2M is around 22:00 LT (01:00 UT), which represents a considerable delay (~ 180 min) with respect to the equatorial onset. The average bubble rise velocity in this case is on the order of 60 m/s, a significant decrease from its solar maximum value. It may be noted further (from Figure 1, right column) that the occurrence percentage of SF over CAJ2M is significantly smaller than that over FZA0M (during both epochs), which is indicative of the fact that only a fraction of the bubble initiated over the equator may develop upward to the apex height of the magnetic field line (about 900 km) crossing the F region over CAJ2M. That fraction decreases significantly from high solar flux to low solar flux epochs especially in the case of strong events.

The color code used in the SF plots in Figure 1 represents the fop values (the top frequency of the SF trace in the ionogram) used to represent the SF intensity as explained in Abdu et al. (2012). We may note the following important features: (1) The duration of SF with higher intensity is largest over FZA0M during 2001. The durations are larger compared to those over CAJ2M. (2) The intensity of SF events over CAJ2M, indicative of that of plasma bubbles, is strikingly more severe during solar maximum than during solar minimum (comparing the fop values in Figure 1, right column). In contrast, (3) the postsunset (and mostly premidnight) SF

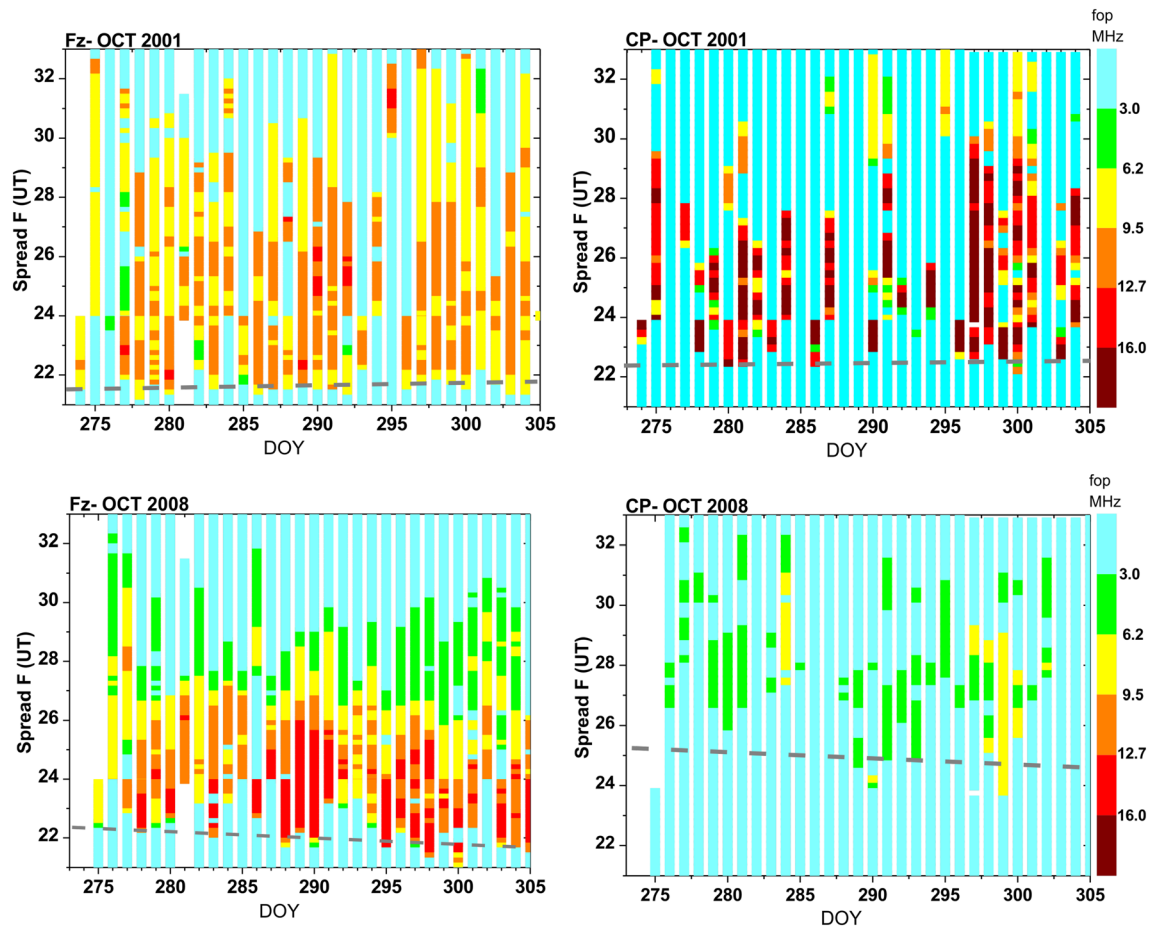


Figure 1. Spread F intensity (represented by the parameter fop) variations with UT (= local time + 3 hr), plotted as a function of the day of the month over Fortaleza and Cachoeira Paulista, Brazil, during October 2001 (top row) and October 2008 (bottom row), representing, respectively, high solar flux ($F_{10.7} = 200$) and low solar flux ($F_{10.7} = 70$) conditions. The average SF onset times are indicated by the dashed near horizontal lines in each panel. The color coding of the fop bins is shown on the right side of the right panels, with background green <3 MHz, dark brown >16 MHz, and intermediate steps.

over FZA0M is as frequent and intense during solar minimum as it is during solar maximum. In fact, there are frequent cases of SF that are more intense during the low solar flux year, 2008, than during the high solar flux year, 2001, (based on the fop values). This last point is of considerable interest and will constitute one of the main focuses of this study.

Figure 2 shows the UT variations in the parameters fop (blue), f_oF2 (pink), and h_mF2 (green) over FZA0M during all days of October for (top) high solar flux (2001) and (bottom) low solar flux (2008) epochs. We may note that the f_oF2 and h_mF2 values are significantly larger during solar maximum than during solar minimum as to be expected based on the correspondingly different solar flux values (representing the respective ionizing EUV radiation). In contrast, the top frequency of the SF trace (fop) that represents the intensity of SF event presents an opposite trend; that is, the bottom-side SF intensity during post sunset hours is generally larger during low solar flux than during high solar flux epoch. Figure 3 brings out this point in terms of the monthly mean values of this parameter. Plotted in this figure are the mean of the fop values over FZA0M and CAJ2M considering (a) the observed cases only (blue curve) as well as (b) the entire 31 days of the month (red curve) for October 2001 and 2008. We may note that (1) over FZA0M the fop mean values during pre-midnight hours, especially, around the peak hours tend to be higher during solar minimum than during maximum in both cases (a) and (b); and (2) over CAJ2M (where the occurrence of SF is representative of that of plasma bubbles), the trend is clearly opposite; that is, the average fop values during high solar flux epoch is significantly higher than that during low solar flux epoch. The latter aspect (point 2) means that the SF associated with developed bubbles is more intense (on an average) during solar maximum than during solar

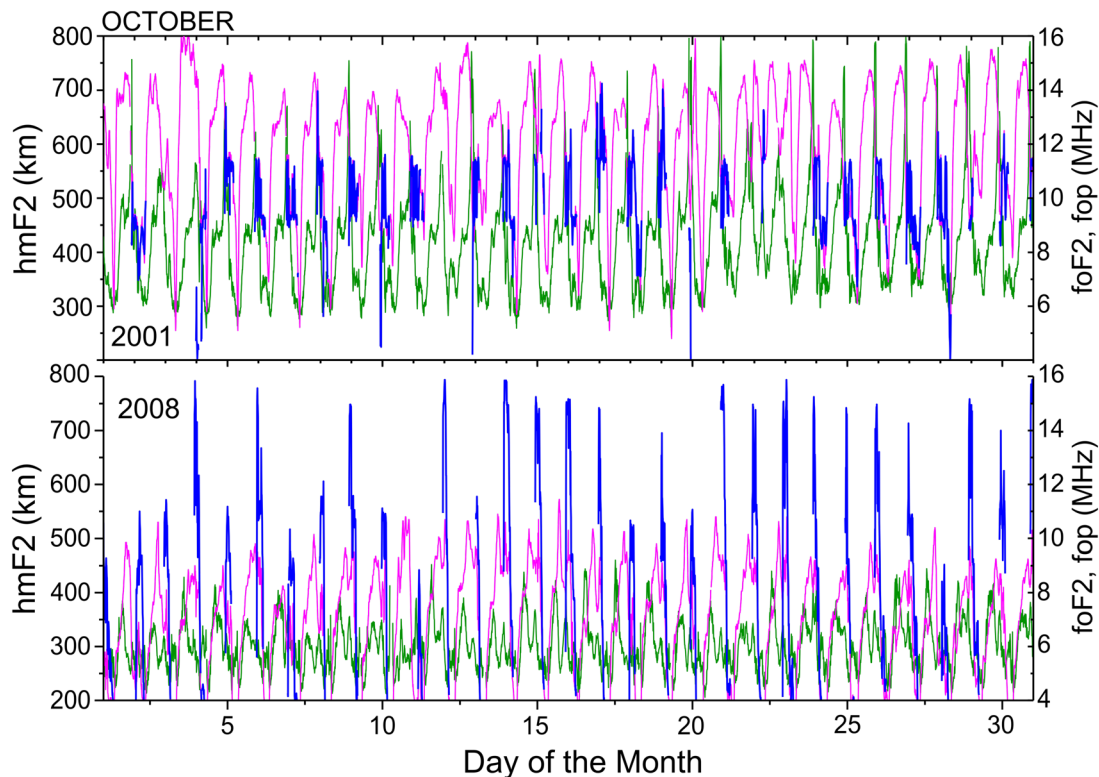


Figure 2. The f_{op} (blue), f_oF_2 (pink), and h_mF_2 (green) parameters for 31 day sequences over Fortaleza during the same periods as in Figure 1. The plots for (top) October 2001 and (bottom) October 2008. Note that the peak values of f_{op} (blue curve) are significantly larger during 2008 than during 2001, but the other two parameters (h_mF_2 and f_oF_2) show an opposite trend (see the text for details).

minimum. This is understandable based also on other observational results. For example, from Jicamarca radar measurements on SF irregularities, Fejer et al. (1999) showed that plume producing intense SF cases corresponded to larger PRE vertical drifts that are typical of higher solar flux values. The new finding here is that the cases of SF that are mostly confined to the bottom side, or associated with very slow bubble growth rate (as can be verified by comparing the two bottom panels in Figure 1) are significantly more intense (at premidnight hours) during solar minimum than during solar maximum. We will discuss below the possible causes of the generation of the more intense (dominantly) bottom-side SF and their much-reduced vertical growth under low solar flux conditions.

3. Discussion

The basic key parameters controlling the ESF/bubble development, as listed above are (1) the PRE vertical drift, (2) evening F layer height, (3) bottom-side density gradient, and (4) seeding source possibly induced by perturbations winds due to gravity waves. We will examine how the PRE vertical drift, and possible seeding sources and variations in their intensity, from solar maximum to minimum epochs could have influenced a corresponding variation in the SF intensity. Figure 4 shows the F layer height oscillations at different plasma frequencies band-pass filtered for the 0.5–1.5 hr period range and the vertical drift variations, for the months of October (left) 2001 and (right) 2008. Gravity wave-induced polarization electric field, presumably arising from perturbations in the wind, produce the oscillations in dhF (as was shown by Abdu et al., 2015). The oscillations in Figure 4 present significant amplitude and occur with a certain degree of phase coherence on all the days as may be noticed in the plot for October 2001 (clearly noticeable at the 8 MHz plasma frequency). The reason for this phase coherence is not clear to us, but we would suggest, for now, the possibility that it could be the result of tidal oscillations producing gravity waves. Since the tidal oscillations do maintain reasonable phase coherence on a day-to-day basis, the gravity waves initiated by such tidal oscillations could also maintain certain day-to-day phase coherence. This cause-effect sequence needs to be developed

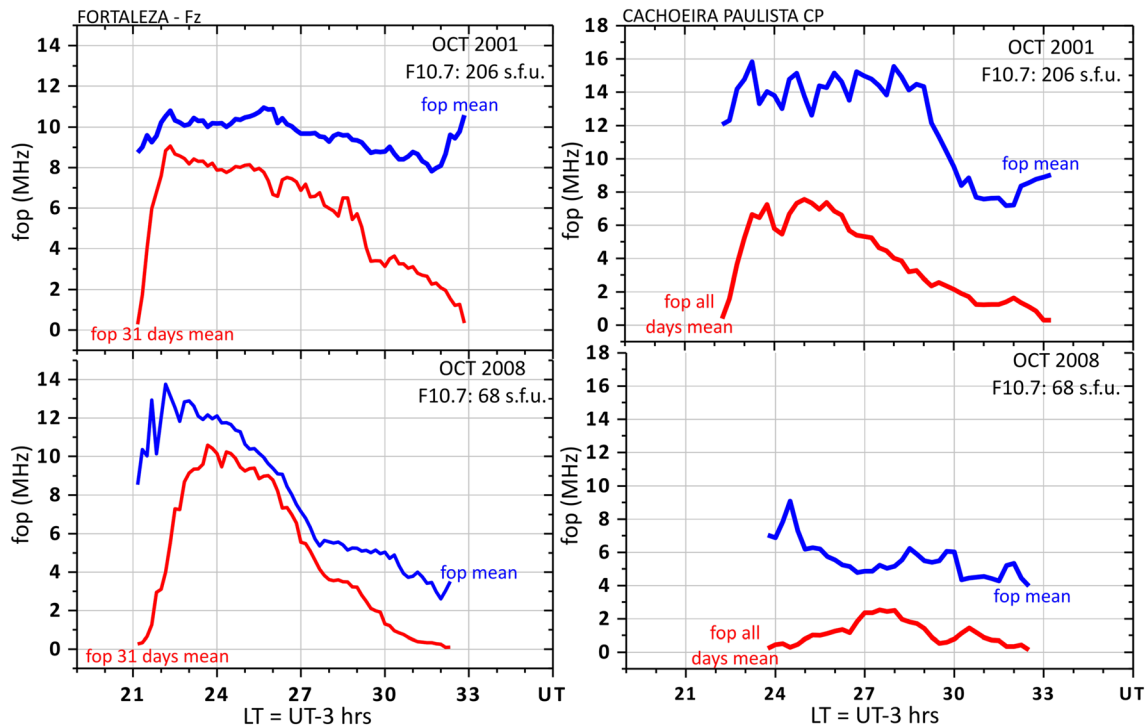


Figure 3. UT variations in the monthly mean values of the fop parameter representing the strength of SF during the October months of 2001 and 2008 over (left) Fortaleza and (right) Cachoeira Paulista. The blue curves represent the mean of all the observed values, and the red curves represent the mean value of the month (i.e., the sum of all fop values divided by the number of days of the month).

further, however. We may further notice that the intensity of these oscillations in the afternoon hours becomes amplified toward sunset, leading to the postsunset ESF irregularity development as indicated by their enhanced amplitudes, shown as the gray segment of the curves starting at around 21:30 UT (18:30 LT). The average PRE vertical drift during October 2001 (Figure 4, bottom left) reached a peak value of about 50 m/s (near 21:30 UT), which is much larger than the threshold value required for bubble growth to the topside ionosphere, statistically known to be above about 35 m/s as found from conjugate point observations in Brazil by Abdu et al. (2009). The ESF intensity index, (represented by the fop parameter), for all running days of October 2001 and 2008, plotted in Figure 2, and the corresponding dhF oscillations and the vertical drifts (for the same days), mass plotted in Figure 4 would suggest that, statistically, the height oscillations, in the presence of the observed vertical drift, were apparently sufficient to account for the SF development, including the associated bubble events, that may have followed.

The dhF fluctuations (at 3 and 6 MHz) (which may also be identified as precursor wave oscillations) and the corresponding vertical drift variations for October 2008 are mass plotted in Figure 4 (right column). They are of significantly smaller amplitude and occur in the height region around 250 km that is well below that of the solar maximum epoch of 2001, which is around 450 km (as will be shown below). These weaker intensity oscillations also evolve into larger amplitude (though to a smaller degree) due to the postsunset SF generation (shown as a gray segment of the curves, in Figure 4, right column). The reason for these oscillations to be of smaller amplitude has to do with the fact that most SF cases over FZAOM are those confined to the F layer bottom side (of limited height extension) only, which do not evolve well into topside bubbles as they did in 2001. This is associated also with the late and weak occurrences of SF over CAJ2M in 2008 (see in Figure 1). The average of the vertical drift velocity prereversal peaks during 2008 is only around 10 m/s (Figure 4, bottom right), which is well below the threshold drift required for SF development. Even the day-to-day deviations in the peak drift that sometimes attain/exceed 20 m/s are unlikely to be sufficient by themselves to explain the occurrence of the relatively more intense SF activity observed over FZAOM during the solar minimum epoch (in Figure 1). In fact, it appears that the approximate positive relationship between the PRE vertical drift and the SF occurrence (or intensity) that generally holds for higher solar flux conditions (not

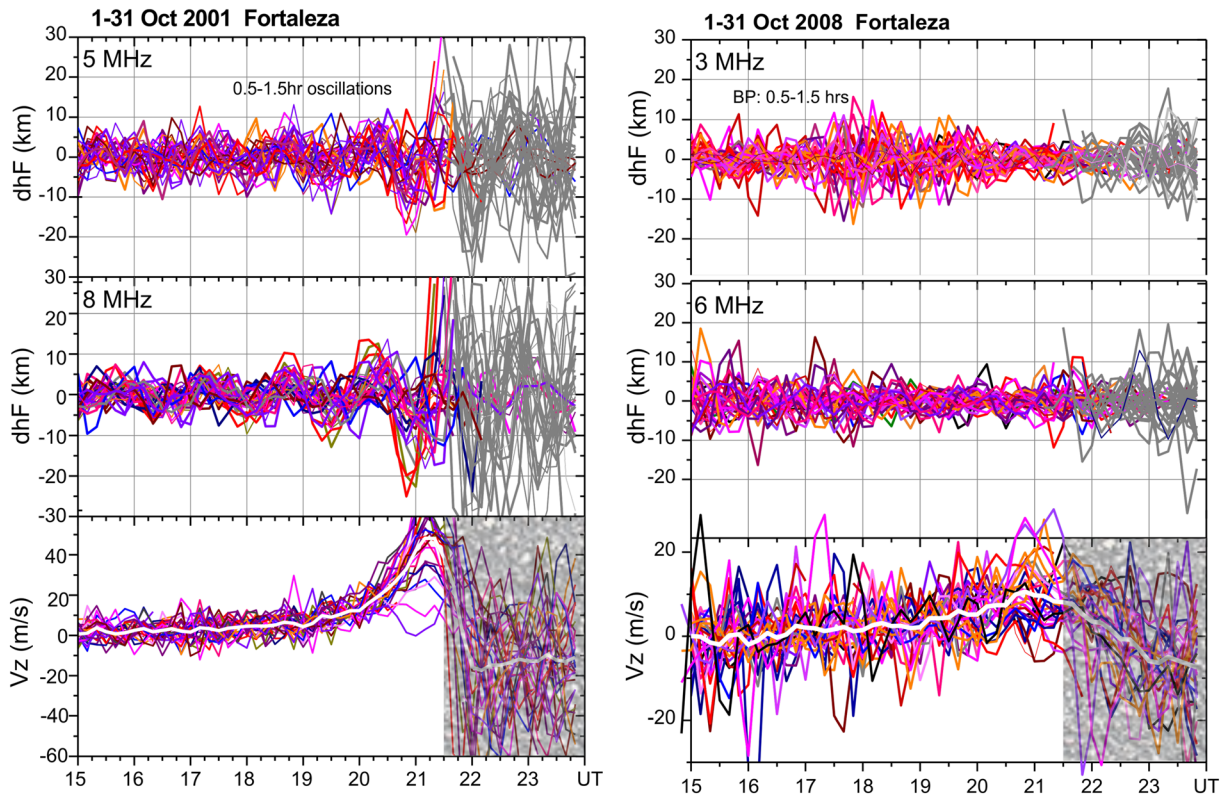


Figure 4. (top and middle rows) Wave oscillations in dhF , band-pass filtered in the 0.5–1.5 hr period range, during 15–24 UT (UT = LT + 3 hr), mass plotted for all days of October. (left column) The results at plasma frequencies of 5 and 8 MHz, are shown for 2001. (bottom row) The corresponding vertical drifts calculated as average of the drifts at four plasma frequencies (5, 6, 7, and 8 MHz), showing also the mean of all days of drift (white superposed curve). (right column) The corresponding plots at plasma frequencies 3 and 6 MHz, and the V_z as mean of the drift at four plasma frequencies (3, 4, 5, and 6 MHz) for 2008.

shown here) do not seem to apply in the same way for solar minimum conditions. The possible factors responsible for the large degree of SF intensity and occurrence rate, observed over FZA0M, during the solar minimum epoch may be examined considering the role of bottom-side density gradient in the generation of these irregularities as discussed below.

Figure 5 shows electron density profiles over FZA0M, for a few quiet days, at the time of the peak in PRE vertical drift during October (right) 2001 and (left) 2008. The SAO Explorer extrapolates the parts of the profiles above the F_2 peak. Our focus is only on the bottom-side upward gradient region of the profiles, which characterizes the semithickness of the layer. We may note that the F layer bottom-side thickness that was around 350 km during 2001 decreased to about 100 km during 2008 with a decrease also in the respective $h_m F_2$ values. This shows that a large increase in the bottom-side gradient, represented by the large decrease in the scale length of the density gradient, occurred from solar maximum to minimum epoch. This variation in the gradient has a significant impact on the instability growth rate terms of Equation 2 arising from both the vertical drift ($V_z = E/B$) term and the gravity (g) term as they transition from solar maximum to minimum years. These growth rate terms can be expressed, for simplicity (and ignoring vertical wind), in terms of their local values, as V_{zp}/L and $g/\nu_{in}L$. The V_{zp} decreases from solar maximum to minimum years causing a corresponding decrease also in the growth rate. However, such a decrease in the growth rate can be offset by the large decrease in the gradient scale length that may also occur simultaneously. The bottom-side density gradient ($L = N/(dN/dhF)$) was calculated for all the density profiles during the months of October 2001 and 2008, and the relationship between all the V_{zp} values and L , considering both the 2001 and 2008 epochs, is shown in Figure 6a, and that between the F layer height and L is shown in Figure 6b. The relationship between the plots in Figures 6a and 6b shows that the F layer uplift caused by the vertical drift (i.e., the V_{zp}) involves a vertical stretching of the layer and not just an uplift of the layer with an unchanging layer

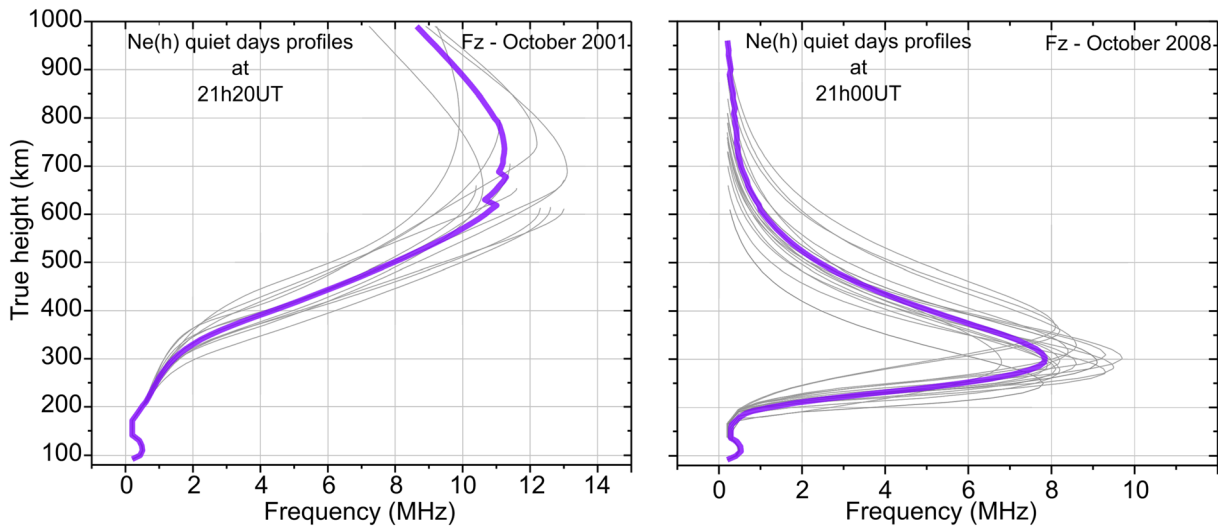


Figure 5. Electron density profiles from Digisonde ionograms at the time of the PRE vertical drift peak (considered as monthly average). The $n(h)$ profiles on individual days as obtained from the SAO Explorer are shown for October (left) 2001 and (right) 2008 over Fortaleza, and their mean profiles are shown as thick curves (in violet color). The legend of the y-axis, that is, “The true height in km”, shown for October 2001 is valid also for 2008.

shape. We note that with an increase in V_{zp} the bottom-side scale length increases almost linearly as does also the F layer height. The increased scale length means a decreased bottom-side gradient that can be effective to retard the bubble growth, while at the same time, the associated height increase may enhance the condition for bubble development. Thus, competing factors are at play in the bubble development phase. Therefore, observational results showing a positive dependence of SF intensity, or occurrence rate, on PRE vertical drift (e.g., Abdu et al., 1983, 2009; Fejer et al., 1999; Kil et al., 2009) necessarily imply the dependence of SF generation on postsunset F layer height and bottom-side density gradient as well, which are largely caused by (or associated with) the V_z variations, whether driven by F layer dynamo, or perhaps by external forcing (through penetration electric field).

The instability growth rate is the sum of the contributions from the key terms of Equation 2 that are interdependent as discussed above. The contribution arising from the term in vertical drift, V_{zp}/L , as a function of the V_{zp} (considering all V_{zp} values observed in 2001 and 2008) is plotted in Figure 7a. For discussion purposes, the V_{zp} values less than ~ 25 m/s may be considered as typical for solar minimum epoch, while the higher values (> 25 m/s) may be considered as representative of solar medium to maximum epoch. We may note in Figure 7a that the growth rate increases rapidly with increase in V_{zp} in its smaller ranges typical of the solar minimum epoch. But for a further increase in V_{zp} (above a transition value $> \sim 25$ m/s) the growth rate tends to flatten (with a few exceptions), which is the result of the gradient scale length increasing (i.e., the density gradient decreasing) with increase in V_{zp} . Thus, an increase in PRE vertical drift (above the transition value), by itself, does not guaranty enhanced SF generation, due to the associated increase occurring also in the gradient scale length. But it may lead to enhanced SF generation as a result of the increase in layer height (due to the V_{zp} increase) and therefore in the gravity term that also increases simultaneously.

The contribution to the instability growth arising from the gravity force term, $g/\nu_{in}L$, is plotted also as a function of F layer height at 5.5 MHz in Figure 7b, separately for 2008 (red curve) and 2001 (blue curve). The ionosphere model by Huba et al. (2000) was used in these calculations. We may note that the growth rate increases with increase in the F layer bottom-side height for both the solar minimum and maximum, which is the result of the increase in the layer height as V_{zp} increases (Figure 7c), accompanied by a decrease in ν_{in} with associated increase in L . It is interesting to note that the instability growth arising from gravity force for smaller V_{zp} values of the solar minimum epoch can be higher than that due to the significantly larger V_{zp} values that characterize the solar maximum epoch. The reason for this is that the gradient length in the term $g/\nu_{in}L$ is significantly smaller during solar minimum than in solar maximum, while the ν_{in} during the two epochs happen to have similar values in their respective height regions. Also plotted in Figure 7c is the

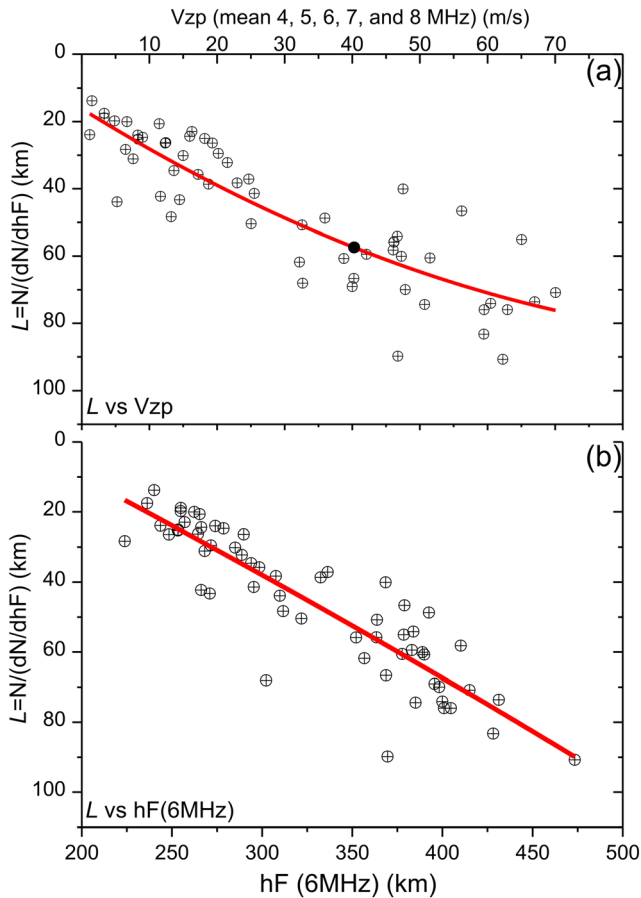


Figure 6. (a) The density gradient scale length ($L = N/(dN/dhF)$) calculated using the difference in true heights between 7 and 4 MHz, plotted as a function of the PRE vertical drift peak (V_{zp}) values considering both the solar flux high (2001) and low (2008) epochs. (b) The same parameter (L) plotted as a function of the hF (6 MHz).

ble extremities to low latitudes on either side of the magnetic equator. Thus, the SF observed over the low-latitude station, CAJ2M, corresponds to a field-aligned bubble structure attaining an apex height of around 900 km over the equator. Accordingly, the observed delay of ~ 1 hr in the SF onset at CAJ2M relative to that at FZA0M could yield an average bubble vertical rise velocity of ~ 150 m/s for October 2001. Again, considering that the height of SF development over FZA0M during October 2008 is around 250 km, the corresponding rise velocity of the bubble/SF observed over CAJ2M can be estimated as ~ 60 m/s. Thus, the average bubble rise velocity during solar minimum is drastically reduced compared to that during solar maximum, even though the (postsunset) SF intensity over FZA0M during the same two epochs is either similar or varied in the opposite sense. This unexpected behavior may be caused by the reduced growth rate and limited height extension attained by the bubble developing under conditions of strong bottom-side gradient and smaller layer thickness as will be examined from an R-T instability growth simulation to be presented below.

It is evident that the main characteristics of the SF and EPB activities during the solar maximum and minimum epochs can be very different due to the background ionosphere exercising different degrees of control on the EPB development during the two epochs. In particular, the EPBs rise to higher apex heights during high solar flux conditions, while they are confined to lower apex heights under low solar flux condition, even though the associated SF intensity in the latter case can be much stronger than that of high solar flux condition. In order to understand such contrasting and varying natures of the ESF characteristics during the two epochs, we carry out a numerical experiments of R-T instability growth rate leading to the formation of

dependence of the F layer height on V_{zp} (the height being at 5.5 MHz plasma frequency, which is the central frequency at which the scale length L was calculated at the time of V_{zp}). The increase in growth rate due to the gravity force term with increase of height and that due to V_{zp} can be easily visualized in this plot.

We may now consider the total growth rate arising from the two terms of Equation 2 (that of the vertical drift ($V_z = E/B$) and that of gravity (g)), for some typical values of PRE vertical drift. For example, at $V_{zp} = 20$ m/s representing the solar minimum epoch, the sum of the two terms comes out to be $\sim 10^{-4} \text{ s}^{-1}$, which corresponds to a growth time of ~ 15 min. If we consider a $V_{zp} = 50$ m/s, the total growth time is also close to the same value (see Table 1 for details). (This is because the gradient length increases with increase of the V_{zp} .) This order of growth time is in good agreement with the usually observed time delay between the peak in the PRE vertical drift and the subsequent onset of SF over the equator (Abdu et al., 1981, 2014). Thus, depending on the variabilities in the V_{zp} values, in the F layer height, and in the ion-neutral collision frequency, during the two epochs, the postsunset SF intensity during solar minimum can be equally intense as, or even more intense than, that of solar maximum epoch, which indeed is the case in the observational data over FZA0M presented here (compare the ESF intensity distributions in Figure 1, left column, during the premidnight hours). The duration of the intense post sunset SF (presenting a rapid decay after midnight) is shorter during 2008 compared to the duration in 2001 (Figure 1). This is due to the significantly lower F layer heights (< 250 km) at these hours in 2008 as compared to the relatively higher F layer heights (~ 350 km) during 2001 (not shown here).

From Figure 1, an average bubble rise velocity can be estimated by considering the delay in the SF onset over CAJ2M in relation to that over FZA0M (see, e.g., Abdu et al., 1983). It is known that bubble development is initiated at about 350 km (at the F layer bottom side) over the equator and that the magnetic field-aligned bubble structure vertically rising over the equator (close to FZA0M) results in a latitudinal extension of the bub-

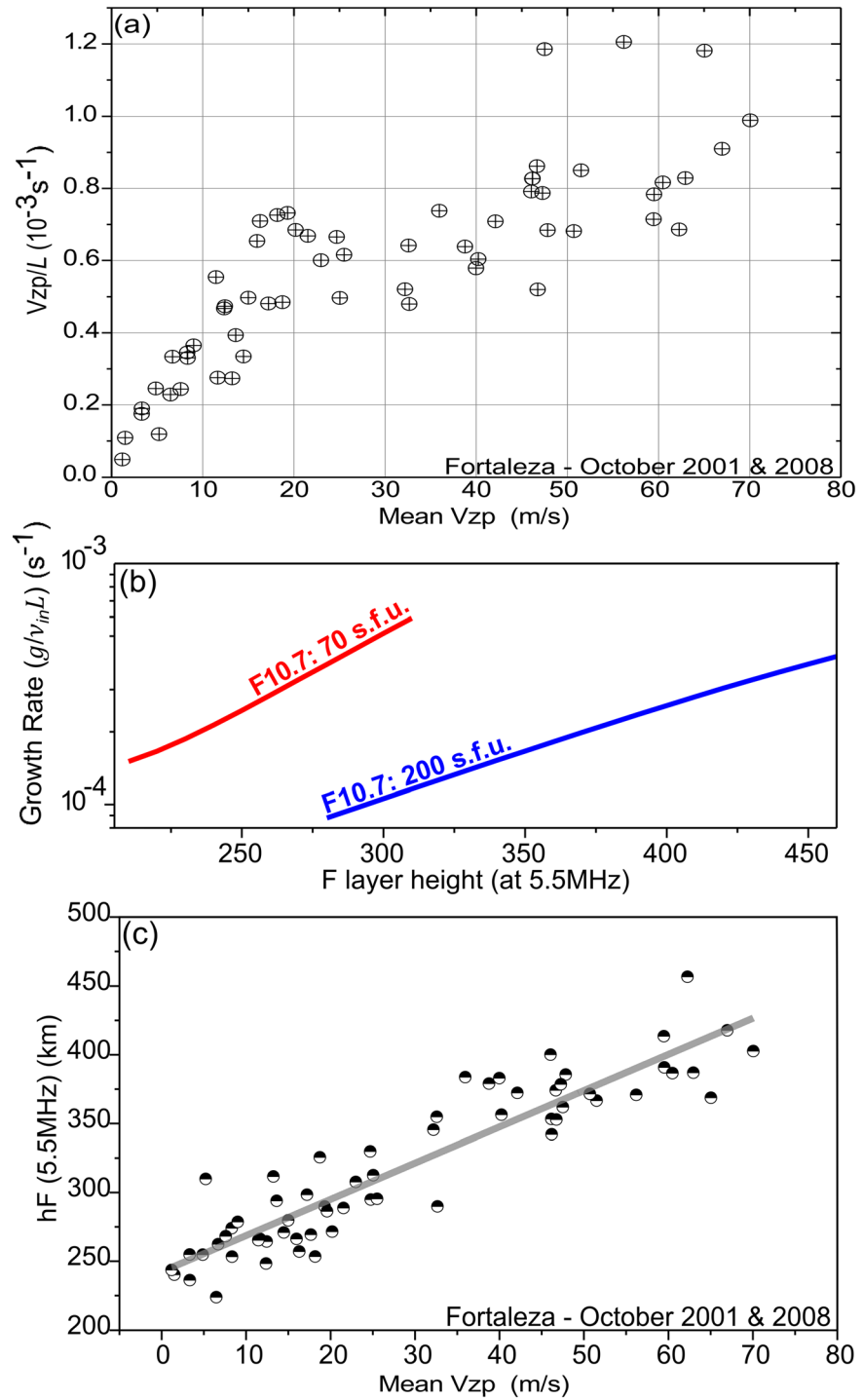


Figure 7. (a) The R-T instability growth rate term (V_{zp}/L) plotted as a function of V_{zp} ; (b) the R-T instability growth rate term, $g/\nu_{in}L$ (due to gravity force, g/ν_{in} , and bottom-side gradient L), as a function of the height at 5.5 MHz plasma frequency, for $F_{10.7} = 70$ (red line) and $F_{10.7} = 200$ (blue curve); and (c) the height at 5.5 MHz plasma frequency versus V_{zp} , considering both 2008 and 2001.

Table 1
The Terms in the R-T Instability Growth Rates Calculated for V_{zp} Values of 20 and 50 m/s

V_{zp} (m/s)	V_{zp}/L (s^{-1})	$g/\nu_{in}L$ (s^{-1})	Total growth rate
20	6×10^{-4}	3.7×10^{-4}	9.7×10^{-4}
50	8×10^{-4}	2×10^{-4}	10×10^{-4}

plasma bubbles, using the simulation code by Kherani et al. (2016). Two numerical experiments (NE1 and NE2) that used different ambient conditions representing the two epochs, notably with respect to the PRE vertical drift, the F layer bottom-side density gradient or the scale length (L_v), and the altitude of the F_{peak} , were performed. They are described as follows:

1. NE1: larger L_v , with higher F_{peak} height and larger PRE vertical drift to represent the high solar flux conditions; and
2. NE2: smaller L_v , with lower F_{peak} height and smaller PRE vertical drift to represent the low solar flux conditions.

The simulation results are presented in Figure 8. Figures 8a and 8b show the time evolution of the plasma updraft (U_m) inside the density depletion and the degree of depletion (dn), respectively, for the NE1 and NE2 cases. Also shown in Figure 8a (dashed lines) are the PRE vertical drift variations used in the simulation. We may note (in Figure 8a) that the nonlinear updraft starts much earlier in the case of NE1 than in NE2. The increase of the updraft follows closer to the time of the peak growth rate γ_m in the NE1 case than it is in the NE2 case. However, the velocity attained at a time (at the end of the simulation) appears higher in the latter case (of low solar flux value). The corresponding degree of depletion (plotted in Figure 8b) has a faster rate of evolution for the NE1 case than for the NE2 case. However, a higher degree of depletion is reached in the solar minimum case (NE2) than in the solar maximum case (NE1) at the end of the simulation time. It is known that a higher degree of depletion could favor generation of more intense irregularities in specific spectral bands. This is an indication that the irregularity strength (as manifested by the strength of SF echoes, corresponding to irregularity scale sizes of tens of meters to kilometers) can be larger for the low solar flux epoch than for high solar flux epoch. The large updraft, exceeding (in some case) two times the peak PRE vertical drift, and the large degree of depletion (dn), exceeding 75% of the background, both having multiexponent growth, represent the nonlinear evolution of R-T instability leading to formation of EPB.

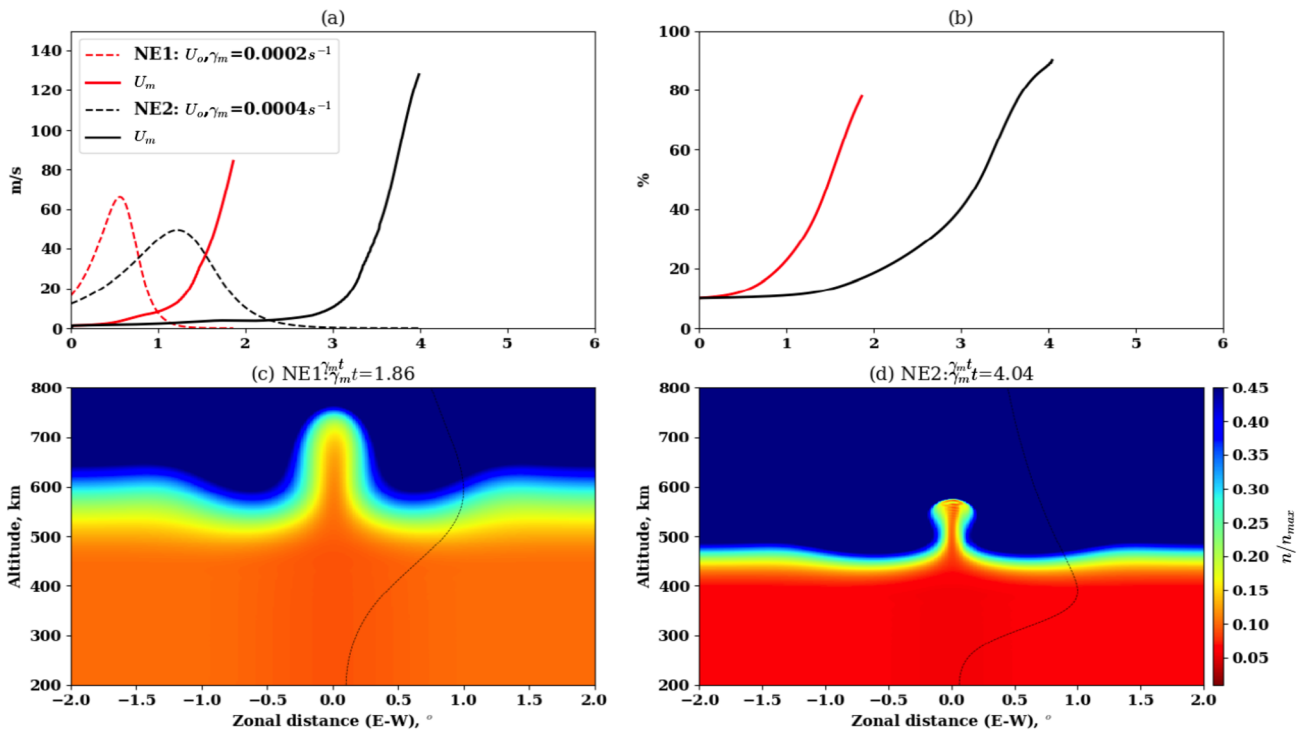


Figure 8. (a) For the NE1-NE2 cases, the time evolution of the plasma updraft (U_m) inside the density depletion for high and low solar flux conditions and (b) the degree of depletion (dn), respectively, for the two cases. (c and d) Iso electron density distribution showing the development and growth of plasma bubble for solar maximum and minimum conditions. Typical vertical density profiles are shown by dotted lines. The sharper density gradient representing the low solar flux condition (in panel d) may especially be noted.

Figures 8c and 8d show plasma density distribution in the form of density isolines depicting a snapshot of the R-T instability evolution phase taken at the times of the peak dn (maximum depletion) that are 155 and 168 min for the NE1 and NE2 cases, respectively. It is evident that EPBs are formed in both the numerical experiments, and they present characteristics that are visibly different in the two cases. In the case of the NE1, the EPB attains a higher apex height (~ 750 km; Figure 8c), while in the NE2 case, the apex height is only ~ 570 km (Figure 8d). It may be noted further that the density gradient at the EPB boundaries (walls) is significantly smaller in the NE1 than in the NE2 case. These gradients are maintained also in the initial bottom-side vertical density gradients of the background plasma in both the cases (as represented by the dashed curves in both Figures 8c and 8d). Thus, we note that in the case of NE2, the degree of depletion is stronger, the updraft velocity is higher, and the density gradient at the EPB wall is stronger, which make it a case of more intense bubble than the EPB in NE1, although the equatorial apex height in the latter is less than that in the former case. It is possible to associate the relatively stronger bubble characteristics of NE2 to the more intense SF events often observed over FZA0M, based on the fop parameter, during the low solar flux epoch (Figure 2). We may further note the following: (1) in the NE1 case the bottom-side gradient region has higher height (~ 350 m) and its width is also larger (~ 220 km), whereas (2) in NE2 the gradient region is at a lower height (~ 250 km) and it has a smaller width (~ 100 km). The simulation results show that the conditions in (1) are conducive for EPB vertical growth to higher apex altitude, which appears to be compatible with the SF occurrence rate observed during the October 2001 epoch over the low-latitude station CAJ2M in Figure 1. During this epoch, the SF, representing the EPB that attains an apex height of >900 km (to be observable over CAJ2M), generally has a higher intensity due to the larger background plasma density of the equatorial ionization anomaly (EIA) crest region, but the occurrence rate is less than that over the equatorial site, FZA0M, because the probability of the EPB attaining high enough apex heights determines the SF occurrence rate over CAJ2M. However, during the low solar flux epoch of October 2008 (in Figure 1) the SF over CAJ2M is more delayed and the occurrence rate significantly smaller as compared to that of October 2001. This is compatible with the conditions for the EPB growth mentioned in item (2) above, according to which the lower height of the instability initiation and the smaller thickness of the gradient region are responsible for the lower apex height reached by the EPB, which therefore becomes sparsely observable from CAJ2M. Thus, the stronger bubble intensity presented by the limited vertical growth during the low solar flux epoch results in a more intense SF observed over FZA0M. When observed over CAJ2M, the intensity of the SF echoes is weaker due to the smaller background plasma density that characterizes the low solar flux epoch. In this way the model experiments (NE1 and NE2) appear to convincingly explain the gross features of the contrasting SF occurrence and intensity observed during high and low solar flux epochs.

4. Conclusions

We have analyzed the Digisonde data from equatorial and low latitude sites in Brazil, in order to study the development of SF irregularities as a function of the leading critical parameters of the postsunset ionosphere that are known to control such development. These parameters are mainly the evening prereversal vertical drift (zonal electric field), the F layer heights, and the bottom-side density gradient. It should be highlighted here that this is the first study of its kind in the literature that addresses the important question concerning the control of the SF development by the F layer bottom-side density gradient. The main objective of the study is to gain an understanding of the ESF development processes that could be helpful for eventual perfection of predictive capability on the occurrence and growth of these irregularities. The analysis was performed for the October months of 2001 and 2008, which correspond to the high and low activity epochs, respectively, of the present solar cycle. The important conclusion from this study may be noted as follows: (1) The basic key parameters controlling ESF/bubble development in the equatorial/low-latitude ionosphere are the PRE vertical drift, the evening F layer height, the bottom-side density gradient (or the scale length $[L_v]$) and the seeding source in the form of perturbation wind or gravity waves; (2) the intensity of these dynamical parameters may undergo a significant decrease from solar maximum to minimum epoch and vice versa; (3) the postsunset ESF over FZA0M has an onset of about 30 min later during solar minimum than during solar maximum years; (4) the intensity of the SF, reckoned by the parameter fop, is significantly higher (by a factor of 2.5) during solar maximum as compared to that of the solar minimum period; (5) On the other hand the cases of SF associated with very slow bubble growth rate or that are confined to bottom-side are significantly more intense (in the pre midnight hours) during solar minimum than during

solar maximum in terms their f_oF_2 values; and (6) the F layer height at fixed plasma frequencies undergo oscillation of 0.5–1.5 hr period with the amplitudes of oscillation progressively increasing toward sunset hours, and in most cases they represent precursors to the post sunset ESF development. These are some of the new findings that emerged from this study, and investigations are being pursued for gaining further clarifications and understanding on these points.

Data Availability Statement

The *Dst/Sym-H* data were downloaded from WDC/Kyoto site at <http://wdc.kugi.kyoto-u.ac.jp/wdc/Sec3.html>. The IMF data were obtained from the website <https://omniweb.gsfc.nasa.gov>. Digisonde data over Sao Luis, Fortaleza, and Cachoeira Paulista were obtained from <https://ulcar.uml.edu/DIDBase/> and <http://www.inpe.br>.

Acknowledgments

The authors acknowledge the support received from the Sao Paulo State Foundation for Promotion of Research (FAPESP) through the Process 2016/24970-7. The authors also acknowledge the support received from the Ministry of Science and Technology and Conselho Nacional de Desenvolvimento Científico e Tecnológico (CNPq) through Process CNPq 300883/2008-0. The authors wish to thank the Coordenação de Aperfeiçoamento de Pessoal de Nível Superior (Capes) for a senior visiting professorship at ITA/DCTA. J. Sousasantos acknowledges FAPESP fellowship under Process 2018/06158-9.

References

- Abdu, M. A., Batista, I. S., & Bittencourt, J. A. (1981). Some characteristics of spread F at the magnetic equatorial station Fortaleza. *Journal of Geophysical Research*, *86*(A8), 6836–6842. <https://doi.org/10.1029/JA086iA08p06836>
- Abdu, M. A., Batista, I. S., Reinisch, B. W., de Souza, J. R., Sobral, J. H. A., Pedersen, T. R., et al. (2009). Conjugate Point Equatorial Experiment (COPEX) campaign in Brazil: Electrodynamics highlights on spread F development conditions and day-to-day variability. *Journal of Geophysical Research*, *114*, A04308. <https://doi.org/10.1029/2008JA013749>
- Abdu, M. A., Batista, I. S., Reinisch, B. W., MacDougall, J. W., Kherani, E. A., & Sobral, J. H. A. (2012). Equatorial range spread F echoes from coherent backscatter, and irregularity growth processes, from conjugate point digital ionograms. *Radio Science*, *47*, RS6003. <https://doi.org/10.1029/2012RS005002>
- Abdu, M. A., de Souza, J. R., Kherani, E. A., Batista, I. S., MacDougall, J. W., & Sobral, J. H. A. (2015). Wave structure and polarization electric field development in the bottomside F layer leading to postsunset equatorial spread F . *Journal of Geophysical Research: Space Physics*, *120*, 6930–6940. <https://doi.org/10.1002/2015JA021235>
- Abdu, M. A., Kherani, E. A., Batista, I. S., Reinisch, B. W., & Sobral, J. H. A. (2014). Equatorial spread F initiation and growth from satellite traces as revealed from conjugate point observations in Brazil. *Journal of Geophysical Research: Space Physics*, *119*, 375–383. <https://doi.org/10.1002/2013JA019352>
- Abdu, M. A., Medeiros, R. T., Sobral, J. H. A., & Bittencourt, J. A. (1983). Spread F plasma bubble vertical rise velocities determined from spaced ionosonde observations. *Journal of Geophysical Research*, *88*(A11), 9197–9204. <https://doi.org/10.1029/JA088iA11p09197>
- Alfonsi, L., Spogli, L., Pezzopane, M., Romano, V., Zuccheretti, E., De Franceschi, G., et al. (2013). Comparative analysis of spread- F signature and GPS scintillation occurrences at Tucumán, Argentina. *Journal of Geophysical Research: Space Physics*, *118*, 4483–4502. <https://doi.org/10.1002/jgra.50378>
- Booker, H. G., & Wells, H. W. (1938). Scattering of radio waves in the F region of ionosphere. *Terrestrial Magnetism and Atmospheric Electricity*, *43*(3), 249–256. <https://doi.org/10.1029/TE043i003p00249>
- Farley, D. T., Balsley, B. B., Woodman, R. F., & McClure, J. P. (1970). Equatorial spread F : Implications on VHF radar observations. *Journal of Geophysical Research*, *75*(34), 7199–7216. <https://doi.org/10.1029/JA075i034p07199>
- Farley, D. T., Bonelli, E., Fejer, B. G., & Larsen, M. F. (1986). The prereversal enhancement of the zonal electric field in the equatorial ionosphere. *Journal of Geophysical Research*, *91*(A12), 13,723–13,728. <https://doi.org/10.1029/JA091iA12p13723>
- Fejer, B. G., Scherliess, L., & de Paula, E. R. (1999). Effects of the vertical plasma drift velocity on the generation and evolution of equatorial spread F . *Journal of Geophysical Research*, *104*(A9), 19,859–19,869. <https://doi.org/10.1029/1999JA900271>
- Fritts, D. C., Abdu, M. A., Batista, I. S., Batista, P. P., Buriti, R. A., Burnside, R., et al. (2009). The spread F Experiment (SpreadFEX): Program overview and first results. *Earth, Planets and Space*, *61*(4), 411–430. <https://doi.org/10.1186/BF03353158>
- Haerendel, G., Eccles, J. V., & Cakir, S. (1992). Theory for modeling the equatorial evening ionosphere and the origin of the shear in the horizontal plasma flow. *Journal of Geophysical Research*, *97*(A2), 1209–1223. <https://doi.org/10.1029/91JA02226>
- Heelis, R. A., Kendall, P. C., Moffet, R. J., Windle, D. W., & Rishbeth, H. (1974). Electrical coupling of the E and F regions and its effect on the F region drifts and winds. *Planetary and Space Science*, *22*(5), 743–756. [https://doi.org/10.1016/0032-0633\(74\)90144-5](https://doi.org/10.1016/0032-0633(74)90144-5)
- Huang, C. S., & Kelley, M. C. (1996). Nonlinear evolution of equatorial spread F : 2. Gravity wave seeding of Rayleigh-Taylor instability. *Journal of Geophysical Research*, *101*(A1), 293–302. <https://doi.org/10.1029/95JA02210>
- Huba, J. D., Joyce, G., & Fedder, J. A. (2000). Sami2 is Another Model of the Ionosphere (SAMI2): A new low-latitude ionosphere model. *Journal of Geophysical Research*, *105*(A10), 23,035–23,053. <https://doi.org/10.1029/2000JA000035>
- Hysell, D. L., Kudeki, E., & Chau, J. L. (2005). Possible ionospheric preconditioning by shear flow leading to equatorial spread F . *Annales Geophysicae*, *23*(7), 2647–2655. <https://doi.org/10.5194/angeo-23-2647-2005>
- Jayachandran, B., Balan, N., Rao, P. B., Sastri, J. H., & Bailey, G. J. (1993). HF Doppler and ionosonde observations on the onset conditions of equatorial spread F . *Journal of Geophysical Research*, *98*(A8), 13,741–13,750. <https://doi.org/10.1029/93JA00302>
- Kherani, E. A., Abdu, M. A., Fritts, D. C., & de Paula, E. R. (2011). The acoustic gravity wave induced disturbances in the equatorial ionosphere. In M. Abdu, & D. Pancheva (Eds.), *Aeronomy of the Earth's atmosphere and ionosphere, IAGA Special Sopron Book Series* (Vol. 2, pp. 141–162). Dordrecht: Springer. https://doi.org/10.1007/978-94-007-0326-1_10
- Kherani, E. A., Bharuthram, R., Singh, S., Lakhina, G. S., & de Meneses, F. C. (2016). Unstable density distribution associated with equatorial plasma bubble. *Physics of Plasmas*, *23*(4), 042901–042905. <https://doi.org/10.1063/1.4945636>
- Kil, H., DeMajistre, M., Paxton, L. J., & Zhang, Y. (2006). F region Pedersen conductivity deduced using the TIMED/GUVI limb retrievals. *Annales Geophysicae*, *24*(5), 1311–1316. <https://doi.org/10.5194/angeo-24-1311-2006>
- Kil, H., Paxton, L. J., & Oh, S.-J. (2009). Global bubble distribution seen from ROCSAT-1 and its association with the evening prereversal enhancement. *Journal of Geophysical Research*, *114*, A06307. <https://doi.org/10.1029/2008JA013672>
- Kudeki, E., Akgiray, A., Milla, M., Chau, J. L., & Hysell, D. L. (2007). Equatorial spread- F initiation: Post-sunset vortex, thermospheric winds, gravity waves. *Journal of Atmospheric and Solar-Terrestrial Physics*, *69*(17–18), 2416–2427. <https://doi.org/10.1016/j.jastp.2007.04.012>

- Li, G., Otsuka, Y., Ning, B., Abdu, M. A., Yamamoto, M., Wan, W., et al. (2016). Enhanced ionospheric plasma bubble generation in more active ITCZ. *Geophysical Research Letters*, *43*, 2389–2395. <https://doi.org/10.1002/2016GL068145>
- MacDougall, J. A., Abdu, M. A., Jayachandran, P. T., Cecile, J. F., & Batista, I. S. (1998). Presunrise spread *F* at Fortaleza. *Journal of Geophysical Research*, *103*(A10), 23,415–23,425. <https://doi.org/10.1029/98JA01949>
- Maruyama, T. (1988). A diagnostic model for equatorial spread *F*, 1, Model description and application to electric field and neutral wind effects. *Journal of Geophysical Research*, *93*(A12), 14,611–14,622.
- McClure, J. P., Sing, S., Bamgboye, D. K., Johnson, F. S., & Kil, H. (1998). Occurrence of equatorial *F* region irregularities: Evidence for tropospheric seeding. *Journal of Geophysical Research*, *103*(A12), 29,119–29,135. <https://doi.org/10.1029/98JA02749>
- Ossakow, S. L. (1981). Spread-*F* theories—A review. *Journal of Atmospheric and Terrestrial Physics*, *43*(5-6), 437–452. [https://doi.org/10.1016/0021-9169\(81\)90107-0](https://doi.org/10.1016/0021-9169(81)90107-0)
- Ossakow, S. L., Zalesak, S. T., McDonald, B. E., & Chaturvedi, P. K. (1979). Nonlinear equatorial spread *F*: Dependence on altitude of the *F* peak and bottomside background electron density gradient scale length. *Journal of Geophysical Research*, *84*(A1), 17–29. <https://doi.org/10.1029/JA084iA01p00017>
- Otsuka, Y., Shiokawa, K., & Ogawa, T. (2002). Geomagnetic conjugate observations of equatorial airglow depletions. *Geophysical Research Letters*, *29*(15), 1753. <https://doi.org/10.1029/2002GL015347>
- Rastogi, R. G., & Woodman, R. F. (1978). Spread *F* in equatorial ionograms associated with reversal of horizontal *F* region electric field. *Annales Geophysicae*, *34*, 31–36.
- Rishbeth, H. (1971). Polarization fields produced by winds in the equatorial *F* region. *Planetary and Space Science*, *19*(3), 357–369. [https://doi.org/10.1016/0032-0633\(71\)90098-5](https://doi.org/10.1016/0032-0633(71)90098-5)
- Shi, J. K., Wang, G. J., Reinisch, B. W., Shang, S. P., Wang, X., Zherebotsov, G., & Potekhin, A. (2011). Relationship between strong range spread *F* and ionospheric scintillations observed in Hainan from 2003 to 2007. *Journal of Geophysical Research*, *116*, A08306. <https://doi.org/10.1029/2011JA016806>
- Su, S.-Y., Chao, C. K., & Liu, C. H. (2008). On monthly/seasonal/longitudinal variations of equatorial irregularity occurrences and their relationship with the post sunset vertical drift velocities. *Journal of Geophysical Research*, *113*, A05307. <https://doi.org/10.1029/2007JA012809>
- Sultan, P. J. (1996). Linear theory and modeling of the Rayleigh-Taylor instability leading to the occurrence of equatorial spread *F*. *Journal of Geophysical Research*, *101*(A12), 26,875–26,891. <https://doi.org/10.1029/96JA00682>
- Takahashi, H., Taylor, M. J., Pautet, P. D., Medeiros, A. F., Gobbi, D., Wrasse, C. M., et al. (2009). Simultaneous observation of ionospheric plasma bubbles and mesospheric gravity waves during the SpreadFEx Campaign. *Annales Geophysicae*, *27*(4), 1477–1487. <https://doi.org/10.5194/angeo-27-1477-2009>
- Tsunoda, R. T. (1981). Time evolution and dynamics of equatorial backscatter plumes, I. Growth phase. *Journal of Geophysical Research*, *86*(A1), 139–149. <https://doi.org/10.1029/JA086iA01p00139>
- Tsunoda, R. T. (2010). On seeding equatorial spread *F* during solstices. *Geophysical Research Letters*, *37*, L05102. <https://doi.org/10.1029/2010GL042576>
- Tulasi Ram, S., Yamamoto, M., Tsunoda, R. T., Chau, H. D., Hoang, T. L., Damtie, B., et al. (2014). Characteristics of large-scale wave structure observed from African and Southeast Asian longitudinal sectors. *Journal of Geophysical Research: Space Physics*, *119*, 2288–2297. <https://doi.org/10.1002/2013JA019712>
- Wang, Z., Shi, J., Torkar, K., Wang, G., & Wang, X. (2014). Correlation between the ionospheric strong range spread *F* and the scintillations observed in Vanimo. *Journal of Geophysical Research: Space Physics*, *119*, 8578–8585. <https://doi.org/10.1002/2014JA020447>
- Woodman, R. F., & La Hoz, C. (1976). Radar observations of *F* region equatorial irregularities. *Journal of Geophysical Research*, *81*(31), 5447–5466. <https://doi.org/10.1029/JA081i031p05447>
- Zalesak, S. T., Ossakow, S. L., & Chaturvedi, P. K. (1982). Nonlinear equatorial spread *F*: The effect of neutral winds and background Pedersen conductivity. *Journal of Geophysical Research*, *87*(A1), 151–166. <https://doi.org/10.1029/JA087iA01p00151>